Directional dependence of AlN intrinsic complex dielectric function, optical phonon lifetimes, and decay channels measured by polarized infrared reflectivity

M. Kazan,[1,a)] S. Pereira,[2] M. R. Correia,[3] and P. Masri[4]
[1]*Laboratoire de Nanotechnologie et d'Instrumentation Optique, ICD, CNRS (FRE2848), Université de Technologie de Troyes, 10010 Troyes, France*
[2]*CICECO, University of Aveiro, 3810-193 Aveiro, Portugal*
[3]*Department of Physics, I3N, University of Aveiro, 3810-193 Aveiro, Portugal*
[4]*Groupe d'Etude des Semiconducteurs, CNRS-UMR 5650, University of Montpellier II, 34095 Montpellier, France*

(Received 17 April 2009; accepted 19 June 2009; published online 24 July 2009)

The directional dependence of AlN intrinsic complex dielectric function, the phonon lifetimes, and decay channels are investigated by means of polarized infrared reflectivity measurements on several facets of self-nucleated wurtzite AlN crystal of high crystalline quality. The measurement technique and the AlN single crystal used have been selected with the purpose to reduce, as much as possible, any instrumental-based effects as well as phonon scattering mechanisms due to defects. The experimental arrangements necessary to detect well-defined crystallographic orientations and phonons are detailed. The dielectric parameters and the phonon lifetimes are precisely determined as functions of the crystallographic direction from a careful Kramers–Kronig and damped Lorentz oscillator analysis. The ordinary ($\varepsilon_{\infty\perp}$) and extraordinary ($\varepsilon_{\infty\parallel}$) high frequency dielectric constants for high quality AlN crystal are found to be 3.93 and 4.05, respectively, and the ordinary ($\varepsilon_{0\perp}$) and extraordinary ($\varepsilon_{0\parallel}$) static dielectric constants are found to be 7.37 and 8.60, respectively. Our values obtained for the pure character phonon lifetimes are in good agreement with Raman measurements when these are obtained with the necessary care to eliminate linewidth broadening due to the finite slit width. The lifetime of a transversal phonon is found to increase with increasing the phonon energy, while that of a longitudinal phonon is found to decrease with increasing the phonon energy. Based on these observations, preferential decay channels for the AlN phonons are estimated. The results show that in the case of AlN, the widely assumed symmetric optical phonon decay into two phonons of lower energy cannot be justified for the zone center longitudinal phonons.
 [DOI: 10.1063/1.3177323]

I. INTRODUCTION

Aluminum nitride (AlN) has recently attracted much attention due to its physical properties which are appropriate for several technological applications. Its wide energy band gap (~6.2 eV at room temperature[1]) is suitable for the manufacturing of deep ultraviolet (UV) photonic devices. Moreover, due to its high thermal conductivity, hardness, and stability at elevated temperatures, AlN is regarded as ideal heat sink operating in harsh environments. All these important properties are found to be strongly dependent on the surface orientation of the crystal of wurtzite structure.[1,2] On the other hand, the design of optoelectronic or photonic devices requires that the material dielectric functions and optical properties be known as precisely as possible. Moreover, it requires a detailed knowledge on the optical phonon decays and lifetimes. In fact, the decay of the optical phonons can contribute significantly to the thermal conductivity of the material-based device,[2,3] and the lifetimes of the optical phonons can determine the hot-phonon effects, which in the case of GaAs, have demonstrated to play a key role in the carrier relaxation.[4] Consequently, a detailed knowledge on the orientation dependent dielectric functions and phonons decay and lifetimes in AlN is of utmost importance for a successful AlN-based device design.

Among the optical measurement techniques, infrared reflectivity analysis is the most quantitative technique because the semiconductor response to an infrared wavelength excitation can be described by simple theories. Line-shape analysis, comparatively rare for photoluminescence and Raman spectroscopy, can often be carried out to yield quantitative results. For this reason, infrared reflectivity from a semiconductor surface has been widely used for a quantitative study of the dielectric functions of semiconductor materials.[5–15] However, so far the dielectric functions reported were deduced either without taking into account the crystal anisotropy[5–9] or only in the directions parallel (extraordinary) and perpendicular (ordinary) to the crystal *c*-axis.[10–15] For the specific case of AlN, the data reported on the dielectric parameters[5–9] disagreed among the different reports. Such disagreement can be explained by different levels of crystallinity in the samples used, since crystal impurities,[16] disorder,[17] strain,[18,19] and different free carrier density[20,21] can affect significantly the dielectric parameters.

The phonon lifetimes are usually measured from the linewidth of their resonance in Raman spectroscopy.[22–26] Different values for the lifetimes of the wurtzite AlN

[a)]Electronic mail: michel.kazan@utt.fr.

TABLE I. Directional dependence of AlN dielectric parameters and phonon lifetimes as deduced from FTIR reflectivity measurements at near normal incidence on self-nucleated AlN facets with different orientations.

Facet orientation	θ (deg)	ε_∞	ε_0	n_∞	ω (cm^{-1})	Γ (cm^{-1})	$\tau\times10^{-12}$ (s)
$\{10\bar{1}0\}$	0.0	4.05	8.60	2.01	610[a]	6.7	0.79
					889[b]	8.8	0.60
$\{10\bar{1}2\}$	47.3	3.98	8.00	1.99	643[a]	6.0	0.88
$\{10\bar{1}3\}$	57.9	3.96	7.74	1.99	653[a]	5.7	0.93
$\{10\bar{1}4\}$	64.1	3.95	7.62	1.99	658[a]	5.5	0.96
{0002}	90.0	3.93	7.37	1.98	669[a]	5.2	1.00
					916[b]	10.4	0.51

[a]Transversal polarization.
[b]Longitudinal polarization.

phonons, propagating either along or perpendicular to the *c*-axis, were deduced from this measurement technique.[27–29] The authors attributed the disagreement between the values reported to different levels of crystal perfection because the phonon decay, or alternatively the phonon lifetime, is due to the combined effect of anharmonic decay, which determines the intrinsic decay, together with the defect scattering.[30–34] In addition to the error on the intrinsic phonon lifetime coming from defect scattering, a relatively large error can also arise due to the Raman instrumental bandpass broadening. The common procedure to circumvent this issue is to fit the Raman line with a Voigt profile, which corresponds to the convolution of a Lorentz phonon peak with the Gaussian instrumental profile. Such strategy is sometimes inappropriate and leads to inaccurate results, particularly when the intrinsic linewidth is comparable to the instrumental broadening.

In the present work we attempt to overcome these issues and provide reliable data on the directional dependence of the intrinsic dielectric functions and phonon lifetimes of AlN free from instrumental line broadening effects and appreciable contribution from lattice imperfections. To measure accurately the directional dependence of the intrinsic complex dielectric function of AlN, we have performed a careful Kramers–Kronig analysis of properly polarized infrared reflectivity measurements on facets of high-quality self-nucleated wurtzite AlN single crystals with different orientations, ranging from an orientation perpendicular to the *c*-axis to an orientation parallel to the *c*-axis.

By accurately measuring the directional dependence of the damping constants of a generalized damped Lorentz oscillator model of self-nucleated AlN single crystal of high crystalline quality, we are able to overcome the large errors on the phonon lifetime values, which arise from the defect scattering and instrumental bandpass broadening, and provide reliable data on the directional dependence intrinsic phonon lifetimes and decays in AlN. The geometrical arrangements necessary to obtain the directional dependence of complex dielectric function and phonon lifetimes from infrared reflectivity measurements are detailed. We also discuss the decay channels for the transversal and longitudinal phonons. We show that in AlN, in contrast to the common view, the zone center longitudinal optical phonons preferably decay into three other phonons of lower energies. Finally, we compare the obtained values to the available reported data.

II. EXPERIMENTAL

The AlN crystal growth was accomplished by sublimation of an AlN charge placed in the hot zone of a tungsten crucible and subsequent condensation of vapor species in a cooler region. The starting material was AlN powder containing 0.5 wt % of Al_2O_3. Prior to use for crystal growth, the powder was resublimed in the growth cell in an atmosphere of high-purity nitrogen. During resublimation, the powder was kept at about 2300 °C. The crucible lid where the material is supposed to be condensed was kept at 2100 °C. The charge of 200 g was completely sublimed during 24 h of holding time. The growth cell was designed in such a way that it facilitates self-nucleation of AlN single crystals on the crucible walls. The details of the growth procedure and the used growth cell are described elsewhere.[35] The AlN single crystal investigated in this work is taken from the crucible walls. It exhibits the natural crystal habit of AlN with many well-developed facets. The areas of these facets are as large as $\sim5\times5$ mm^2. Further descriptions of the self-nucleated AlN single crystal investigated are provided in Ref. 36. X-ray diffraction measurements allowed the detection of the $\{10\bar{1}0\}$, $\{10\bar{1}2\}$, $\{10\bar{1}3\}$, $\{10\bar{1}4\}$, and {0002} self-nucleated wurtzite AlN facets, which are selected for the infrared reflectivity measurements. The angles (θ) between these facets and the *c*-axis are given in Table I. The surface of each fact was chemically polished immediately prior to its measurement to remove possible contribution from surface oxidation. This self-nucleated AlN single crystal is of high crystalline quality and would provide the intrinsic properties of the material. In order to highlight the high crystalline quality of the self-nucleated AlN single crystal, we illustrate in Fig. 1 its E_2 (high frequency) Raman-active mode line together with that of a typical seeded AlN single crystal. The E_2 mode line is orientation independent and thus, its position and linewidth should provide qualitative information on the crystalline quality, independent of the crystal orientation. The E_2 linewidth of the seeded AlN single crystal is larger than that of the self-nucleated AlN single crystal. This indicates that the phonon-point-defect scattering rate in the seeded AlN single crystal is much higher than that in the self-nucleated AlN single crystal. On the other hand, the E_2 line of the seeded AlN single crystal presents a blueshift relative to that of the self-nucleated AlN single crystal. This

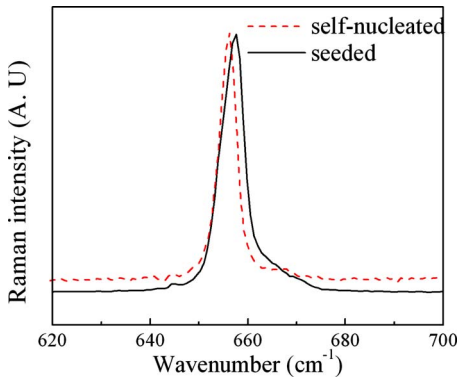

FIG. 1. (Color online) Comparison between the E_2 (high frequency) Raman-active mode line of self-nucleated AlN single crystal (red dashed line) and that of typical seeded AlN single crystal (black solid line). The E_2 line of the typical seeded AlN single crystal presents signatures of point defects (broadness) and defect-induced stress (blueshift), which are not present in the self-nucleated AlN single crystal.

blueshift might be a signature of defect-induced stress in the seeded AlN single crystal, which does not exist in the self-nucleated AlN single crystal.

The infrared reflectivity measurements were performed on the selected self-nucleated AlN facets at near normal incidence ($<5°$ uncertainty) in the 600–7000 cm^{-1} frequency range. A DTGS detector and a KBr beamsplitter were used. The reflectivity from each facet was compared to that of a gold-coated mirror with a reflectivity above 0.98 in the infrared region.[37] The Fourier transform infrared (FTIR) spectrometer used supplies a microscope which allows normal incidence measurements of the reflectivity from the selected facets. Note that the normal incidence reflectivity measurements of crystal facets differing in their orientation are equivalent to the measurements of the reflectivity from facets oriented parallel and perpendicular to the c-axis under different angles of incidence.[38]

Considering x, y, and z as the laboratory coordinate system, a light polarizer was used to polarize the light in the xz (Es) (s-polarized) or in the zy plane (Ep) (p-polarized). In Fig. 2 we schematize the experimental arrangements of our

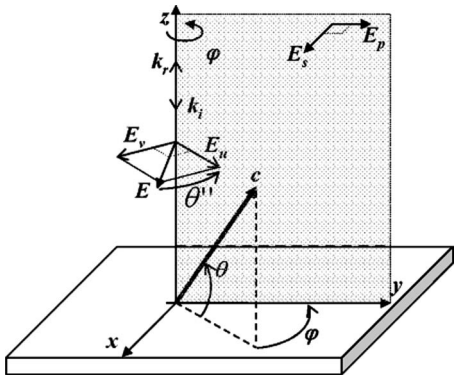

FIG. 2. The experimental arrangements for the infrared reflectivity measurements. The laboratory coordinate system is x, y, and z. The c-axis forms with the measured facet an angle θ and with the zy plane an angle φ. E_s and E_p correspond to light polarization in the zx and zy planes, respectively. It is assumed that in the case of an arbitrary light polarization the electric field splits into two components parallel (E_u) and perpendicular (E_v) to the plane defined by the c-axis and the light wave vector.

measurements. The c-axis forms with the facet an angle θ and with the zy plane an azimuthal angle φ. A goniometer is used for fine variation in the angle φ to make the crystal c-axis lying in well-selected vertical space plane. By this way we were able to manage that Ep and Es are either parallel or perpendicular to the plane defined by the c-axis and the incident light wave vector $\vec{k}_i$. The importance of such control for the present study is discussed in Sec. III.

III. RESULTS AND DISCUSSION

A. Polarization of the light electric field

The effects of the AlN crystal orientation on the *unpolarized* infrared reflectivity spectrum have been previously observed[36] and described.[39] The forms of the ordinary ($\varepsilon_\perp$) and extraordinary ($\varepsilon_\parallel$) dielectric functions have been taken as given by the classical Lorentz-oscillator model

$$\varepsilon_{\perp(\parallel)}(\omega) = \varepsilon_{\infty\perp(\parallel)} + \sum_j \frac{S_{j\perp(\parallel)}\omega^2_{\mathrm{TO}j\perp(\parallel)}}{\omega^2_{\mathrm{TO}j\perp(\parallel)} - \omega^2 - i\Gamma_{j\perp(\parallel)}\omega}, \tag{1}$$

where the indices $\parallel$ and $\perp$ are related to the phonon polarized parallel and perpendicular to the c-axis, respectively, ε_∞ is the high frequency dielectric constant, and S is the oscillator strength equal to $\varepsilon_0 - \varepsilon_\infty$, with ε_0 as the static dielectric constant. The Γ are the transversal phonon damping constants. The summation is over j, which is an index labeling the phonon mode. In the case of AlN, we have one mode in the direction parallel to the c-axis and one mode in the direction perpendicular to the c-axis. Hence, for AlN $j=1$ for both $\varepsilon_\parallel(\omega)$ and $\varepsilon_\perp(\omega)$. Here, we do not take into account the contribution of the free carriers to the lattice dielectric function because it is negligible in a wide band gap material such as AlN. In the case of phonon propagating between the c-axis and the basal plane, the dielectric function can be written in the following form:

$$\varepsilon(\omega,\theta') = \frac{\varepsilon_\perp(\omega)\varepsilon_\parallel(\omega)}{\varepsilon_\perp(\omega)\sin^2\theta' + \varepsilon_\parallel(\omega)\cos^2\theta'}, \tag{2}$$

and the expression for the reflectivity becomes

$$R = \left|\frac{\sqrt{\varepsilon(\omega,\theta')} - 1}{\sqrt{\varepsilon(\omega,\theta')} + 1}\right|^2, \tag{3}$$

where θ' is the angle between the c-axis and the surface normal. It is equal to $\pi/2 - \theta$.

Next, the complex coefficient $r(\omega) = E_r/E_i$, which is defined at the surface as being the ratio between the reflected and incident electric fields, can be rewritten assuming that the infrared response is the combination of the reflected electric field individual components, parallel (E_r^u) and perpendicular (E_r^v) to the plane defined by the c-axis and the light wave vector

$$r(\omega) = \frac{E_r^u\cos(\theta')}{E_i} + \frac{E_r^v\sin(\theta')}{E_i}. \tag{4}$$

As shown in Fig. 2, θ'' is the angle between the total reflected electric field and the plane defined by the c-axis and the light wave vector. Consequently, omitting the term containing the

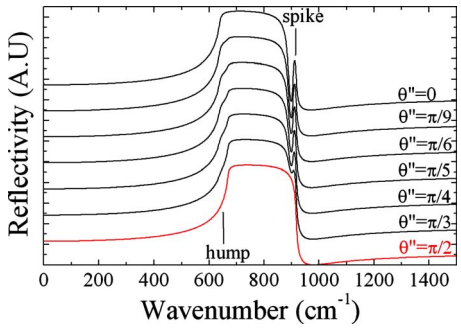

FIG. 3. (Color online) Calculated infrared reflectivity spectra for several values of the angle between the light electric field and the plane defined by the *c*-axis and the light wave vector.

scalar product of the two orthogonal vectors E_r^u and E_r^v, the total reflectivity $R=|r(\omega)|^2$ can be written in the following form:

$$R(\omega) = R_u(\omega)\cos^2(\theta'') + R_v(\omega)\sin^2(\theta''). \quad (5)$$

The terms R_u and R_v are the contributions to the reflectivity which correspond to E_r^u and E_r^v, respectively. It is clear from Eq. (5) that when unpolarized light is used, the infrared reflectivity exhibits contributions from phonon propagating in the plane defined by the *c*-axis and the light wave vector and from other phonon propagating perpendicularly to this plane. Thus, the corresponding dielectric function *cannot* reveal the dielectric function of a specific orientation. On the other hand it can be readily noticed from Eqs. (1)–(5) that the dielectric function in the plane defined by the *c*-axis and the incident light wave vector *can* be deduced from the reflectivity spectrum, without any foreign contribution, when the light electric field is polarized parallel to the plane defined by the *c*-axis and the incident light wave vector (the angle θ'' vanishes). Eventually, the ordinary dielectric function can be deduced from the reflectivity spectrum when the light electric field becomes perpendicular to the plane defined by the *c*-axis and the incident light wave vector ($\theta''=\pi/2$).

The first question can be raised here: how can we polarize the light electric field parallel and perpendicular to the plane defined by the *c*-axis and the light wave vector? To answer this question let us first simulate the reflectivity spectrum of AlN facet with arbitrary crystal orientation for several values of θ'' between 0 and $\pi/2$ by using Eqs. (1)–(5), which describe a generalized damped Lorentz oscillator model. From the results shown in Fig. 3, it can be observed that for θ'' other than $\pi/2$ the infrared reflectivity spectrum shows a hump at the lowest edge or/and a spike at the highest edge of the reststrahlen band. For $\theta''=\pi/2$, the hump and spike vanish completely. The origin of these crystal orientation dependent spectrum features can be comprehended from the solution of Maxwell equation for an electric field propagating in a dielectric medium. Resonances in the reflectivity spectrum occur when the incoming frequency matches the frequency of transverse phonon modes, and vanished dielectric function is the condition for longitudinal phonon modes to exist. This means that the hump and spike are the consequence of the light interaction with anisotropic medium. The hump occurs near the frequency of an additional transverse

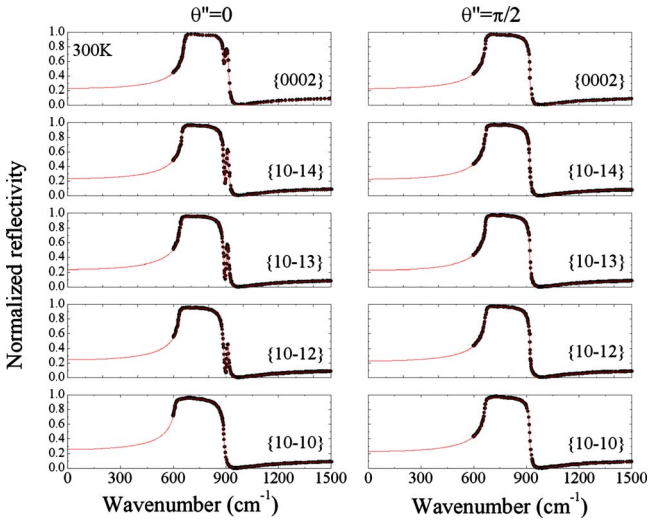

FIG. 4. (Color online) Symbols: measured infrared reflectivity spectra of several AlN self-nucleated facets. The infrared reflectivity spectrum corresponding to $\theta''=0$ and $\theta=90.00$ exhibits weak peak at the highest edge of the reststrahlen band because of the uncertainty on the normal incidence. Solid lines: calculated infrared reflectivity spectra by using the deduced values in an angle dependent generalized damped Lorentz-oscillator model. The excellent agreement between the calculated and measured spectra proves the reliability of the experimental approach and the deduced values.

phonon mode, and the spike originates from additional minimum in the reflectivity spectrum which reveals additional longitudinal phonon mode. The vanishing of both the hump and the spike indicates that the light is interacting with phonons propagating in an isotropic plane. This implies that when the light electric field becomes perpendicular to the plane defined by the *c*-axis and the light wave vector (allowing the detection of the pure ordinary ray) the infrared reflectivity spectrum should not exhibit a spike or hump. Thus, in order to detect the ordinary ray alone, we have used the following experimental procedure. First, we polarize the light electric field in the *zx* plane. Next, we adjust the azimuthal angle φ progressively until the hump and spike in the infrared reflectivity spectrum vanish completely, which according to Fig. 3 corresponds to the situation where $\theta''=\pi/2$. As discussed earlier, this experimental arrangement allows detecting the reflectivity of the pure ordinary ray alone and consequently allows the ordinary dielectric function to be deduced. To obtain the dielectric function in the plane defined by the *c*-axis and the incident light wave vector from the reflectivity spectrum, we keep φ as found in the previous procedure and simply polarize the light in the orthogonal plane (i.e., the anisotropic plane labeled as *zy* in Fig. 2).

B. Directional dependence of the dielectric function

The measured infrared reflectivity spectra from the $\{10\bar{1}0\}$, $\{10\bar{1}2\}$, $\{10\bar{1}3\}$, $\{10\bar{1}4\}$, and {0002} self-nucleated wurtzite AlN facets for $\theta''=0$ and $\theta''=\pi/2$ are presented in Fig. 4 as symbols. The measurements were performed in 600–7000 cm^{-1} frequency range to ensure a reliable Kramers–Kronig analysis, which requires integration in a wide frequency range. However, we illustrate the infrared spectra only in 600–1500 frequency range with the intention

to show in more detail the influence of the crystal orientation on the reststrahlen band features. It can be well observed that when the light electric field is polarized parallel to the plane defined by the *c*-axis and the incident light wave vector ($\theta''=0$) the infrared reflectivity spectrum depends strongly on the crystal orientation. In contrast, when the electric field is polarized perpendicular to the plane defined by the *c*-axis and the incident light wave vector ($\theta''=\pi/2$), the infrared reflectivity spectrum is insensitive to the crystal orientation.

In order to deduce the AlN complex dielectric function parallel and perpendicular to the *c*-axis as well as at several angles θ from the *c*-axis, we have analyzed the infrared reflectivity spectra presented in Fig. 4 by using the Kramers–Kronig technique. In this technique the complex coefficient $r(\omega)$, which is equal to $\sqrt{\varepsilon(\omega)}-1/\sqrt{\varepsilon(\omega)}+1$, is written as a function of the amplitude $\rho(\omega)$ and phase-shift $\phi(\omega)$,

$$r(\omega)=\rho(\omega)\exp[i\phi(\omega)]. \tag{6}$$

The amplitude and phase shift can be expressed as functions of the reflectivity only as

$$\rho(\omega)=\sqrt{R(\omega)}, \tag{7}$$

$$\phi(\omega)=-\frac{1}{2\pi}\int_0^{\infty}\ln\left|\frac{\Omega+\omega}{\Omega-\omega}\right|\frac{d}{d\Omega}[\ln R(\Omega)]d\Omega. \tag{8}$$

From Eqs. (6)–(8) we can see that the Kramers–Kronig technique permits, at each frequency, the determination of the real (ε_1) and imaginary (ε_2) parts of the complex dielectric function from the measured reflectivity data only without the use of any fitting parameters. As can be noticed from Eq. (8), the frequency range where the reflectivity is constant does not contribute to the Kramers–Kronig integral and can be omitted. Also, the frequency ranges where $\Omega \ll \omega$ or $\Omega \gg \omega$ do not contribute significantly because in these regions the term $\ln|\Omega+\omega/\Omega-\omega|$ becomes very weak inside the Kramers–Kronig integral. We therefore believe that the frequency range in which we performed the infrared reflectivity measurements is enough to provide a reliable Kramers–Kronig analysis of the infrared reflectivity in the phonon region.

For an accurate implementation of the Kramers–Kronig integral given in Eq. (8) we have used the following procedure. First, we write Eq. (8) as

$$\phi(\omega)=-\frac{1}{2\pi}\left\{\int_0^1 d\Omega+\cdots\int_{\Omega_i-1}^{\Omega_i}d\Omega+\int_{\Omega_i}^{\Omega_i+1}+\cdots\int_{\Omega_f-1}^{\Omega_f}d\Omega\right\}, \tag{9}$$

where Ω_i and Ω_f correspond to a frequency in the measured frequency range and the frequency where the reflectivity spectrum becomes completely flat, respectively. Next, in each interval $[\Omega_i-1;\Omega_i]$ of 1 cm^{-1} (the resolution of the spectrometer used) we approximate the reflectivity by a linear fit. Then, we obtain $\phi(\omega)$ by solving each integral $\int_{\Omega_i-1}^{\Omega_i}d\Omega$ numerically using the recursive adaptive Simpson quadrature method.[40]

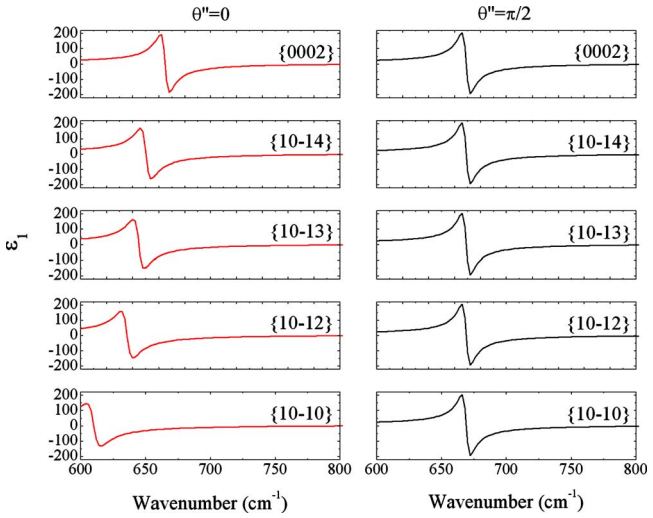

FIG. 5. (Color online) Real part of the complex dielectric functions deduced from the infrared reflectivity spectra for $\theta''=0$ and $\theta''=\pi/2$ and several values of θ.

The real and imaginary parts of the AlN complex dielectric function as functions of the crystal orientation for $\theta''=0$ and $\theta''=\pi/2$ deduced from the Kramers–Kronig analysis are presented by solid lines in Fig. 5 and symbols in Fig. 6, respectively. For $\theta''=\pi/2$, we are always measuring the ordinary complex dielectric function $\varepsilon_{\perp}(\omega)$ whatever the crystal orientation is. Thus, we do not observe orientation dependency in the ordinary dielectric function. However, for $\theta''=0$, we are measuring the dielectric function in the anisotropic plane defined by the *c*-axis and the incident light wave vector, where mixed character phonons of energies depending on the angle between the phonon propagation direction and the *c*-axis influence strongly the dielectric function.[41] When the crystal orientation changes, the angle between the *c*-axis and the direction in which we measure changes, which explains the changes observed in the measured dielectric function.

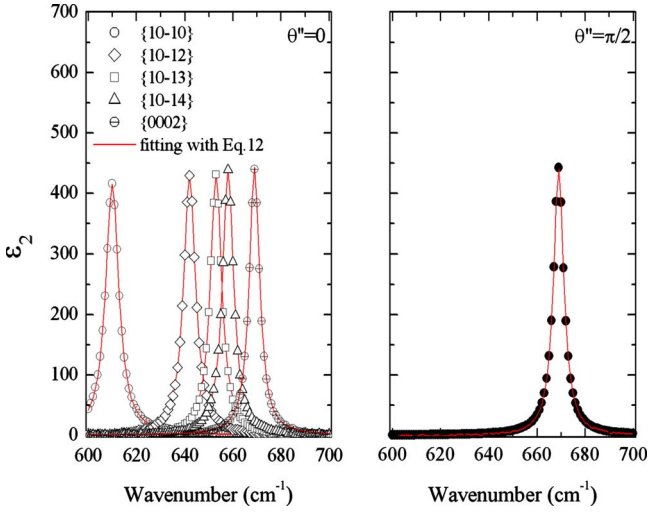

FIG. 6. (Color online) Imaginary part $\varepsilon_2(\omega)$ of the complex dielectric functions for $\theta''=0$ and $\theta''=\pi/2$ and several values of θ. Symbols: as deduced from a careful Kramers–Kronig analysis of the infrared reflectivity spectra. Solid lines: best fit of Eq. (12) to the $\varepsilon_2(\omega)$ obtained from the Kramers–Kronig analysis of the infrared reflectivity data.

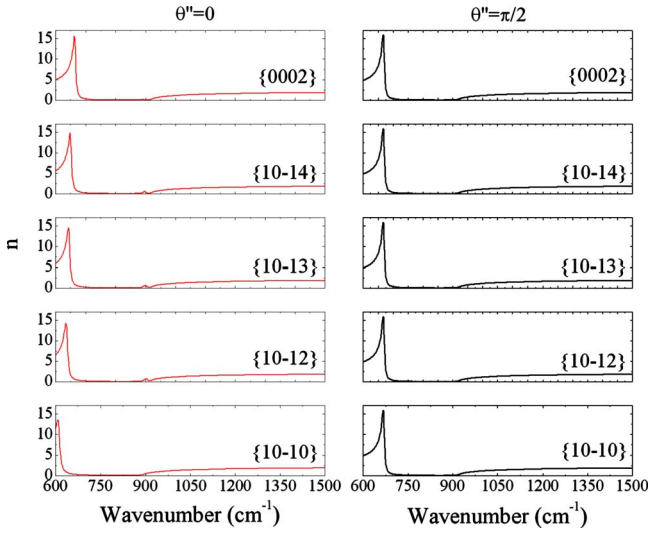

FIG. 7. (Color online) Refractive indices for $\theta''=0$ and $\theta''=\pi/2$ and several values of θ.

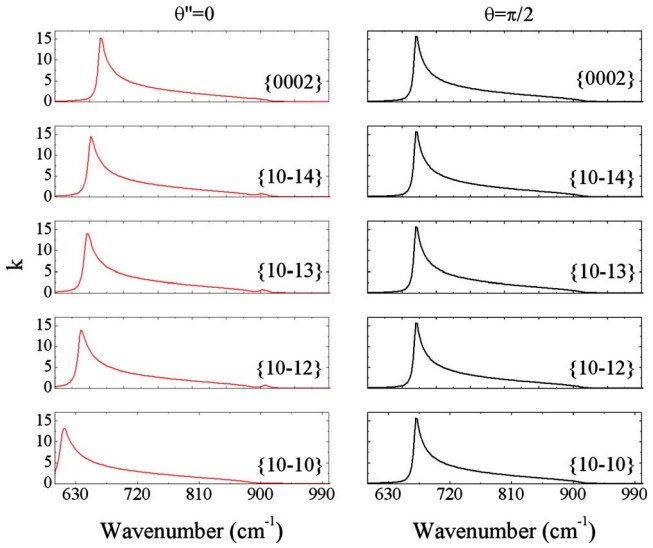

FIG. 8. (Color online) Extinction coefficient for $\theta''=0$ and $\theta''=\pi/2$ and several values of θ.

The high frequency dielectric constants (ε_∞) in the directions parallel and perpendicular to the c-axis as well as at several angles θ from the crystal c-axis are obtained from the corresponding dielectric functions at high frequency, where these dielectric functions become completely flat. The results are presented in Table I.

The deduction of the static dielectric function (ε_0) from the common extrapolation of the real part of the complex dielectric function to zero would provide a relatively wide range of uncertainty because the experimentation limits are often well above the zero frequency. Thus, the directional dependence of ε_0 will be deduced later by following the other procedure.

From the knowledge on the real and imaginary parts of the dielectric function we deduced the refraction index (n) and extinction coefficient (k) as functions of the crystal orientation by using the following relationship:

$$\frac{\sqrt{\varepsilon}-1}{\sqrt{\varepsilon}+1}=\frac{n+ik-1}{n+ik+1}. \tag{10}$$

The results are plotted in Figs. 7 and 8, respectively. The refractive index curves at high frequency allowed deducing the refractive index at high frequency n_∞ as a function of the crystal orientation. The values obtained are given in Table I.

C. Directional dependence of the phonon lifetimes

The maxima of the imaginary parts (ε_2) of the dielectric functions in Fig. 6 are important spectral features. They define the frequencies of the infrared active transversal phonons which interact with the incident light. Thus, as can be noticed from Fig. 6, when the light is polarized perpendicular to the plane defined by the c-axis and the incident light wave vector ($\theta''=\pi/2$), the light interacts with transversal phonon of pure E_1 character propagating perpendicularly to the c-axis, whatever the crystal orientation is. However, when the light electric field is polarized parallel to the plane defined by the c-axis and the incident light wave vector ($\theta''=0$), the incident light interacts with a transverse phonon of A_1-E_1 mixed character propagating at an angle θ from the c-axis.[41] The frequency of this transversal mixed character phonon depends on θ according to Loudon[42] approximation. We give in Table I the frequencies of the transversal pure and mixed character phonons detected by the infrared reflectivity measurements. The results verify Loudon approximation and agree with previously reported results on the orientation dependent transversal phonon frequency in AlN.[41,43]

The orientation dependent energy loss function $[\mathrm{Im}(-1/\varepsilon)]$ for both cases $\theta''=0$ and $\theta''=\pi/2$ is plotted in Fig. 9 by using symbols. As can be observed, for $\theta''=0$ the energy loss function exhibits two peaks. The frequencies of these two peaks are independent from the facet orientation, but their relative intensities are not. For $\theta=\pi/2$ the high frequency peak is relatively very intense compared to the low frequency peak, which is barely seen. The intensity of the high frequency peak decreases with θ while that of the

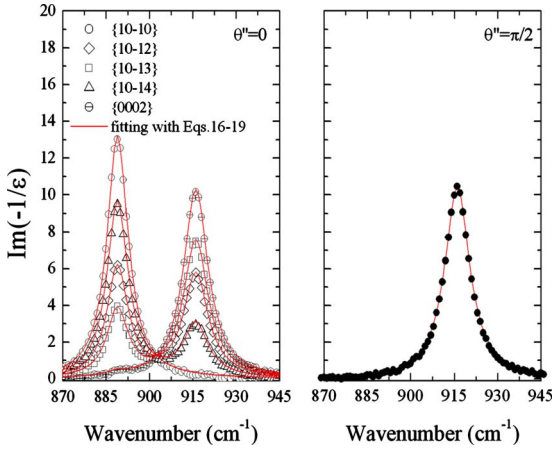

FIG. 9. (Color online) Phonon energy loss function $[\mathrm{Im}(-1/\varepsilon)]$ for $\theta''=0$ and $\theta''=\pi/2$ and several values of θ. Symbols: as deduced from a careful Kramers–Kronig analysis of the infrared reflectivity spectra. Solid lines: best fit of Eq. (19) to the $[\mathrm{Im}(-1/\varepsilon)]$ obtained from the Kramers–Kronig analysis of the infrared reflectivity data.

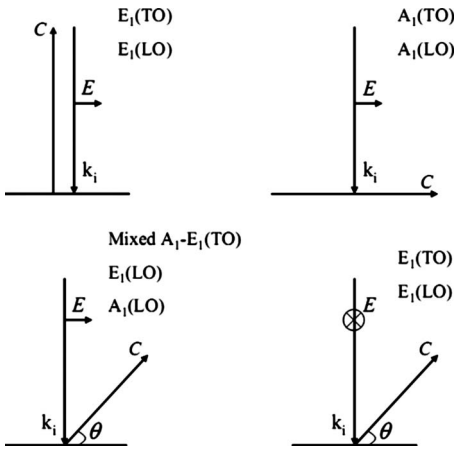

FIG. 10. Normal incidence infrared reflectivity diagrams for a variety of crystal orientations and for *s*- and *p*-polarizations. The allowed phonon modes are indicated near the respective diagram.

low frequency peak increases. For $\theta=0$ the high frequency peak vanishes completely and the low frequency peak becomes very intense. On the other hand, the ordinary ($\theta''=\pi/2$) phonon energy loss function exhibits only one peak insensitive to the crystal orientation. These maxima of the phonon energy loss functions mirror which longitudinal phonons interact with the incident light and suggest the following. When $\theta''=0$, the incident light may interact with one or two longitudinal phonons of *pure* character. The strengths of the signatures of these pure character phonons in the reflectivity spectrum depend on the facet orientation. This is due to a possible splitting of E_p into one component along the *c*-axis direction and another one along the perpendicular direction within the *zy* plane (see Fig. 2). We give in Table I the frequencies of the longitudinal pure character phonons detected by the infrared reflectivity measurements. In Fig. 10 we summarize schematically which phonons can be detected from the infrared reflectivity in both cases $\theta''=0$ and $\theta''=\pi/2$ for various facet orientations.

After identifying the symmetry of the detected AlN phonons and determining their frequencies, let us estimate their intrinsic lifetimes from our infrared reflectivity measurements. For a given angle θ, the real $[\varepsilon_1(\omega)]$ and the imaginary $[\varepsilon_2(\omega)]$ parts of the dielectric function in the case of a single resonance are given by

$$\varepsilon_{1\theta}(\omega)=\varepsilon_{\infty}+\frac{(\varepsilon_{0\theta}-\varepsilon_{\infty\theta})\omega_{\mathrm{TO}\theta}^2(\omega_{\mathrm{TO}\theta}^2-\omega^2)}{(\omega_{\mathrm{TO}\theta}^2-\omega^2)^2+\omega^2\Gamma_{\mathrm{TO}\theta}^2} \tag{11}$$

and

$$\varepsilon_{2\theta}(\omega)=\frac{(\varepsilon_{0\theta}-\varepsilon_{\infty\theta})\omega_{\mathrm{TO}\theta}^2\Gamma_{\mathrm{TO}\theta}\omega}{(\omega_{\mathrm{TO}\theta}^2-\omega^2)^2+\Gamma_{\mathrm{TO}\theta}^2\omega^2}. \tag{12}$$

This can be readily demonstrated from a complete separation between the real and the imaginary parts of Eq. (1). On the other hand, as demonstrated previously from the Kramers–Kronig analysis, the imaginary part of the dielectric function exhibits only one peak (single resonance) which shifts in frequency with varying the angle θ. Thus, the imaginary part of the dielectric function deduced from the Kramers–Kronig analysis can be described by Eq. (12). This serves to deduce accurately the two unknown parameters $\varepsilon_{0\theta}$ and $\Gamma_{\mathrm{TO}\theta}$ in Eq. (12) by performing a systematic variation in $\varepsilon_{0\theta}$ and $\Gamma_{\mathrm{TO}\theta}$ to achieve the best representation (solid lines in Fig. 6) of the $\varepsilon_2(\omega)$ obtained. As can be noticed from Eq. (12), the parameter $\varepsilon_{0\theta}$, which is proportional to the oscillator strength *S*, influences mainly the intensity of $\varepsilon_2(\omega)$, while the damping constant $\Gamma_{\mathrm{TO}\theta}$ influences mainly the linewidth of $\varepsilon_2(\omega)$ peak. Note that in the fitting of Eq. (12) to the $\varepsilon_2(\omega)$ obtained, the angle θ is also adjusted slightly to account for the uncertainty on the normal incidence. This step is used in adjusting the position of the synthesized $\varepsilon_2(\omega)$ peak relative to that obtained from the Kramers–Kronig analysis. The deduced values of $\varepsilon_{0\theta}$ and $\Gamma_{\mathrm{TO}\theta}$ for all the crystal orientations investigated are given in Table I. The lifetime of the transversal phonon propagating at an angle θ from the *c*-axis can then be estimated from the corresponding damping constant $\Gamma_{\mathrm{TO}\theta}$ (which can be considered as an energy uncertainty similar to the linewidth of the Raman resonance) by using the energy-time uncertainty relation

$$\frac{\Gamma}{\hbar}=\frac{1}{\tau}. \tag{13}$$

Here $\hbar$, the reduced Planck constant, is equal to 5.3×10^{-12} cm^{-1} s. The obtained values of the lifetimes of the transversal phonons detected by the infrared reflectivity measurements are given in Table I.

The procedure previously described serves to detect the lifetimes of the pure and mixed character *transversal* phonons, since the damping constants involved in the equations are those of transversal phonons propagating at different angles from the *c*-axis. In order to deduce the lifetimes of the pure character *longitudinal* phonons, instead of using the summation model of a damped oscillator given in Eq. (1) to describe the dielectric functions in the directions parallel and perpendicular to the *c*-axis, we use the factorized model of a damped oscillator

$$\varepsilon_{\|(\perp)}(\omega)=\varepsilon_{\infty}\prod_j\frac{\omega_{\mathrm{LO}j\|(\perp)}^2-\omega^2-i\Gamma_{\mathrm{LO}j\|(\perp)}\omega}{\omega_{\mathrm{TO}j\|(\perp)}^2-\omega^2-i\Gamma_{\mathrm{TO}j\|(\perp)}\omega}, \tag{14}$$

which involves the damping constants of the pure character longitudinal phonons $\Gamma_{\mathrm{LO}\|(\perp)}$. As mentioned previously, for the case of AlN $j=1$. The use of the equivalence between Eq. (1) and Eq. (14) permits the determination of the generalized Lyddane–Sachs–Teller (GLST) relation[44]

$$\frac{\varepsilon_0}{\varepsilon_{\infty}}=\frac{\omega_{\mathrm{LO}}^2+\frac{\Gamma^2}{4}}{\omega_{\mathrm{TO}}^2+\frac{\Gamma^2}{4}}. \tag{15}$$

For $\Gamma_{\mathrm{TO}\theta}=0$ Eq. (15) reduces to the well known Lyddane–Sachs–Teller relation.[45]

The real part of the dielectric function given by Eq. (10) can be written as

$$\varepsilon_{1\|(\perp)}(\omega) = \varepsilon_{\infty\|(\perp)} \frac{(\omega_{\mathrm{LO}\|(\perp)}^2 - \omega^2)(\omega_{\mathrm{TO}\|(\perp)}^2 - \omega^2) + \Gamma_{\mathrm{LO}\|(\perp)}\Gamma_{\mathrm{TO}\|(\perp)}\omega^2}{(\omega_{\mathrm{TO}\|(\perp)}^2 - \omega^2)^2 + \Gamma_{\mathrm{TO}\|(\perp)}^2\omega^2} \tag{16}$$

and its imaginary part can be written as

$$\varepsilon_{2\|(\perp)}(\omega) = \varepsilon_{\infty\|(\perp)} \frac{\Gamma_{\mathrm{TO}\|(\perp)}\omega(\omega_{\mathrm{LO}\|(\perp)}^2 - \omega^2) - \Gamma_{\mathrm{LO}\|(\perp)}\omega(\omega_{\mathrm{TO}\|(\perp)}^2 - \omega^2)}{(\omega_{\mathrm{TO}\|(\perp)}^2 - \omega^2)^2 + \Gamma_{\mathrm{TO}\|(\perp)}^2\omega^2}. \tag{17}$$

On the other hand, the dielectric function $\varepsilon(\omega, \theta')$ of an anisotropic crystal, which is a function of the angle between the c-axis and the surface normal θ', is given by Eq. (2). By converting θ' to θ ($\theta' = \pi/2 - \theta$) its real $[\varepsilon_1(\omega, \theta)]$ and imaginary $[\varepsilon_2(\omega, \theta)]$ parts can be written as

$$\varepsilon_1(\omega, \theta) = \frac{(\varepsilon_{1\perp}\varepsilon_{1\|} - \varepsilon_{2\perp}\varepsilon_{2\|})(\varepsilon_{1\perp}\cos^2\theta + \varepsilon_{1\|}\sin^2\theta)}{(\varepsilon_{1\perp}\cos^2\theta + \varepsilon_{1\|}\sin^2\theta)^2 + (\varepsilon_{2\perp}\cos^2\theta + \varepsilon_{2\|}\sin^2\theta)^2} + \frac{(\varepsilon_{1\perp}\varepsilon_{2\|} + \varepsilon_{1\|}\varepsilon_{2\perp})(\varepsilon_{2\perp}\cos^2\theta + \varepsilon_{2\|}\sin^2\theta)}{(\varepsilon_{1\perp}\cos^2\theta + \varepsilon_{1\|}\sin^2\theta)^2 + (\varepsilon_{2\perp}\cos^2\theta + \varepsilon_{2\|}\sin^2\theta)^2} \tag{18}$$

and

$$\varepsilon_2(\omega, \theta) = \frac{(\varepsilon_{1\perp}\varepsilon_{2\|} + \varepsilon_{1\|}\varepsilon_{2\perp})(\varepsilon_{1\perp}\cos^2\theta + \varepsilon_{1\|}\sin^2\theta)}{(\varepsilon_{1\perp}\cos^2\theta + \varepsilon_{1\|}\sin^2\theta)^2 + (\varepsilon_{2\perp}\cos^2\theta + \varepsilon_{2\|}\sin^2\theta)^2} - \frac{(\varepsilon_{1\perp}\varepsilon_{1\|} - \varepsilon_{2\perp}\varepsilon_{2\|})(\varepsilon_{2\perp}\cos^2\theta + \varepsilon_{2\|}\sin^2\theta)}{(\varepsilon_{1\perp}\cos^2\theta + \varepsilon_{1\|}\sin^2\theta)^2 + (\varepsilon_{2\perp}\cos^2\theta + \varepsilon_{2\|}\sin^2\theta)^2}. \tag{19}$$

By substituting Eqs. (16) and (17) in Eqs. (18) and (19), we obtain for any value of θ the real and imaginary parts of the dielectric function as functions of the pure character longitudinal phonon damping constants $\Gamma_{\mathrm{LO}\|(\perp)}$. Now, for a given value of θ, $\Gamma_{\mathrm{LO}\|(\perp)}$ are the only unknown parameters in the equations of the real and imaginary parts of the dielectric function. The values of $\Gamma_{\mathrm{LO}\|(\perp)}$ for AlN can then be determined accurately by varying systematically $\Gamma_{\mathrm{LO}\|}$ and $\Gamma_{\mathrm{LO}\perp}$ to achieve with the same values the best representation (solid lines in Fig. 9) of the energy loss function curves obtained from the Kramers–Kronig analysis for all the values of θ investigated. The obtained values of $\Gamma_{\mathrm{LO}\|}$ and $\Gamma_{\mathrm{LO}\perp}$ are given together with the corresponding phonon lifetimes estimated from Eq. (13) in Table I.

The parameters of the generalized damped Lorentz-oscillator model given in Table I as functions of the crystal orientation were used to calculate the orientation dependent infrared reflectivity spectra by using Eqs. (1)–(5). The result of this calculation is shown in Fig. 4 as solid lines. The excellent agreement between measured and synthesized infrared reflectivity spectra proves the reliability of the deduced parameters given in Table I.

D. Discussion and comparison with previous results

The characteristics of the detected phonons presented in Table I show that the lifetime of a transversal phonon increases with increasing its energy. However, the opposite behavior occurs for a longitudinal phonon; its lifetime decreases with increasing its energy. To interpret the trends of the lifetimes of the transversal and longitudinal phonons, two important characteristics of the wurtzite-type structure should be taken into account. First, in the wurtzite-type structure the electric field stiffens the force constant of the phonon and thereby raises the frequency of the longitudinal phonon over that of a transversal phonon. Second, the electrostatic forces dominate over the anisotropy in the short-range forces, which results in that the longitudinal-transversal splitting becomes larger than the A_1-E_1 splitting. These two characteristics make the energies of all the pure and mixed character transversal phonons relatively much lower than the energies of the longitudinal phonons.[41] Based on this, the trends of the lifetimes of the transversal and longitudinal phonon can suggest the following. Due to the small gap between the acoustic and optical phonon bands in AlN and due to its low energy,[46] the zone center transversal optical phonon decays into two acoustic phonons with conserving the energy and momentum (for the zone center phonons the Umklapp process is disregarded). With increasing its energy, the transversal phonon finds fewer channels to decay into two other acoustic phonons and does not have sufficient energy to decay into three other acoustic phonons, which implies an increase in its lifetime. However, due to its relatively high energy, the longitudinal phonon can decay into two acoustic phonons, one acoustic and one optical phonon of lower energy, or three acoustic phonons. When its energy increases, the decay probability into optical phonons of lower energies or three acoustic phonons becomes more favorable, and consequently its lifetime decreases. These results clearly show that despite the small energy gap between the acoustic and optical phonon branches, the widely used Klemens model[47] which assumes a symmetric decay of the zone center optical phonon into two other phonons of lower energy cannot describe the longitudinal optical phonon decay in AlN. Model involving four-phonon normal processes or the quartic anharmonic instead of the cubic anharmonic term would be more appropriate to account for the longitudinal optical phonon decay at the zone center in AlN.

TABLE II. AlN dielectric parameters as deduced previously.

$n_{\parallel}$	$n_{\perp}$	$\langle n_{\infty} \rangle$	$\varepsilon_{0\parallel}$	$\varepsilon_{0\perp}$	$\langle \varepsilon_0 \rangle$	Ref.
2.09	2.04		9.32	7.76		15[a]
2.17	2.12		8.12	7.87		34[b]
		1.9			7.0	6
		1.99			7.72	7
		2.11			8.68	8
		2.114			8.713	9
			8.9	8.3		50
		2.2			9.14	5

[a]Obtained from a theoretical approach.
[b]Obtained from measurements on samples highly contaminated by oxygen.

Let us now consider the dielectric parameters deduced in previous works in Table II. As can be noticed, they are different from the dielectric parameters deduced here. For instance, the value of the ordinary static dielectric parameter $\varepsilon_{0\perp}$ deduced here is 7.37 lower than all of the previously reported values. The value of the extraordinary static dielectric function $\varepsilon_{0\parallel}$ deduced in this work is 8.6 between the lowest[34] and the highest reported values.[15] The values of the ordinary and extraordinary high frequency dielectric parameters are both lower than all of the previously reported values. It is important to note that although our data for the dielectric parameters are deduced independently, either from the Kramers–Kronig analysis or from the damped Lorentz oscillator model, they match very well with the GLST relation given in Eq. (15). This, along with the fact that our infrared measurements were performed on high crystalline quality and well oriented single crystal AlN facets, provides strong support to the reliability of the AlN parameters reported here.

In Table III, we show the previously reported values for phonon lifetimes of pure character. These values have been deduced from Raman spectroscopy. The values for low frequency phonons obtained by fitting the Raman line with a Lorentz peak[33] corrected by assuming a well-defined value for the instrumental bandpass,[29] or by fitting the Raman line with the Voigt profile[28] or according to Posener tables[27,48] (when the signal-to-noise ratio does not allow fitting with Voigt profile), are relatively higher than those deduced in this work. However, because of the issues discussed in Sec. I, the fit of the Raman line with Voigt profile and according to Posener tables (which are established from approximated methods of computing the Voigt profile) often provides inaccurate values for the phonon lifetime. Moreover, the fit of the Raman line with a Lorentz peak is inadequate to provide accurate values for the phonon lifetimes. On the other hand, the value for the lifetime of the transversal phonon propagating in the direction perpendicular to the *c*-axis and the values of the lifetimes of the transversal and longitudinal phonons propagating in the direction parallel to the *c*-axis deduced in this work compare well with those reported in Ref. 49, where systematic Raman measurements of the phonon lifetimes have been made. These Raman measurements were performed by acquiring the Raman spectra at successive slits, plotting the measured linewidth values as functions of the slit width, then extrapolating to the zero slit to obtain actual phonon linewidths with good precision. The agreement between the values obtained from this work and those obtained from Ref. 49 adds further support to the reliability of our approach and to the results obtained, including the trends of the lifetimes of the transversal and longitudinal phonons, which are used to estimate the possible phonon decay channels in AlN. It is worth to note here that the described reflectivity measurements involving the temperature factor would lead to a better understanding of the optical phonon decay channels in AlN, in which their knowledge is very important for a thermal-management strategy.

IV. CONCLUSION

The directional dependence of the intrinsic AlN complex dielectric function, optical phonon lifetimes, and decay channels has been investigated. In order to overcome the instrumental and phonon-defect scattering errors and provide reliable experimental data, we have employed a careful Kramers–Kronig analysis of polarized infrared reflectivity data from several facets of high-quality self-nucleated AlN single crystal. The experimental geometries necessary to allow the light polarization in well-defined crystal directions are detailed. The ordinary and extraordinary dielectric parameters as well as the dielectric parameters for several AlN crystallographic directions in the anisotropic plane could be measured with high precision. The energies and the lifetimes of the transversal and longitudinal pure or mixed character infrared-active phonons could be detected and allow the estimation of the possible decay channels in AlN. The values deduced for the phonon lifetimes were found to be in good

TABLE III. Energies and lifetimes of the zone center optical phonons propagating parallel and perpendicular to the *c*-axis as deduced previously. We show only values obtained at room temperature.

(Symmetry E_1)[a] (cm^{-1})				(Symmetry A_1)[b] (cm^{-1})				
ω_{TO}	Γ_{TO}	ω_{LO}	Γ_{LO}	ω_{TO}	Γ_{TO}	ω_{LO}	Γ_{LO}	Ref.
667.2	2.9	909.6	7.5	608.5	4.5	888.9	7.3	33
668	5.8			608	7.0	890	11.9	49
						889	9	29
669	3.5	916		610	4.0	889	10.5	28
						889	9.3	27

[a]Symmetry E_1 designates a phonon propagating perpendicular to the *c*-axis.
[b]Symmetry A_1 designates a phonon propagating along the *c*-axis.

agreement with those deduced from Raman scattering measurements when appropriate care is taken to eliminate the instrumental broadening effects on the Raman linewidths. Our results are expected to stimulate further investigations of the optical phonon decay channels, in which their knowledge is important to gain insight into the effects of the anharmonic terms of the interatomic forces.

ACKNOWLEDGMENTS

We acknowledge the financial support by FCT, Portugal (Grant Nos. BPD/39121/2007 and PTDC/FIS/65233/2006). Also, we would like to thank Erlangen University (UEMIMS6 group) for providing samples.

[1]A. Sedhain, N. Nepal, M. L. Nakarmi, T. M. Al tahtamouni, J. Y. Lin, H. X. Jiang, Z. Gu, and J. H. Edgar, Appl. Phys. Lett. **93**, 041905 (2008).
[2]M. Kazan, S. Pereira, M. R. Correia, and P. Masri, Phys. Rev. B **77**, 180302 (2008).
[3]M. Kazan, S. Pereira, J. Coutinho, M. R. Correia, and P. Masri, Appl. Phys. Lett. **92**, 211903 (2008).
[4]*Proceedings of the Seventh International Conference on Hot Carriers in Semiconductors*, edited by C. Hamaguchi and M. Inoue (Hilger, London, 1992).
[5]A. T. Collins, E. C. Lightowlers, and P. J. Dean, Phys. Rev. **158**, 833 (1967).
[6]Y. Zhiqiang and G. L. Harding, Thin Solid Films **120**, 81 (1984).
[7]T. L. Chu and R. W. Kelm, J. Electrochem. Soc. **122**, 995 (1975).
[8]C. J. Kubiak, C. R. Aita, F. S. Hickernell, and S. J. Joseph, Mater. Res. Soc. Symp. Proc. **4**, 775 (1985).
[9]S. Loughin and R. H. French, in *Handbook of Optical Constants of Solids III*, edited by E. D. Palik (Academic, New York, 1998), pp. 373–401.
[10]M. Kazan, L. Ottaviani, E. Moussaed, R. Nader, and P. Masri, J. Appl. Phys. **103**, 053707 (2008).
[11]N. Ashkenov, B. N. Mbenkum, C. Bundesmann, V. Riede, M. Lorenz, D. Spemann, E. M. Kaidashev, A. Kasic, M. Schubert, M. Grundmann, G. Wagner, H. Neumann, V. Darakchieva, H. Arwin, and B. Monemar, J. Appl. Phys. **93**, 126 (2003).
[12]A. Kasic, M. Schubert, T. Frey, U. Köhler, D. J. As, and C. M. Herzinger, Phys. Rev. B **65**, 184302 (2002).
[13]S. Shokhovets, O. Ambacher, B. K. Meyer, and G. Gobsch, Phys. Rev. B **78**, 035207 (2008).
[14]M. Schubert, T. E. Tiwald, and C. M. Herzinger, Phys. Rev. B **61**, 8187 (2000).
[15]W. J. Moore, J. A. Freitas, Jr., R. T. Holm, O. Kovalenkov, and V. Dmitriev, Appl. Phys. Lett. **86**, 141912 (2005).
[16]G. Leibiger, V. Gottschalch, A. Kasic, and M. Schubert, Appl. Phys. Lett. **79**, 3407 (2001).
[17]J. Sik, M. Schubert, G. Leibiger, V. Gottschalch, and G. Wagner, J. Appl. Phys. **89**, 294 (2001).
[18]T. Hofmann, G. Leibiger, V. Gottschalch, I. Pietzonka, and M. Schubert, Phys. Rev. B **64**, 155206 (2001).
[19]V. Darakchieva, J. Birch, M. Schubert, T. Paskova, S. Tungasmita, G. Wagner, A. Kasic, and B. Monemar, Phys. Rev. B **70**, 045411 (2004).
[20]A. Kasic, M. Schubert, S. Einfeldt, D. Hommel, and T. E. Tiwald, Phys. Rev. B **62**, 7365 (2000).
[21]A. Kasic, M. Shubert, Y. Saito, Y. Nanishi, and G. Wagner, Phys. Rev. B **65**, 115206 (2002).
[22]T. R. Hart, R. L. Aggarwal, and B. Lax, Phys. Rev. B **1**, 638 (1970).
[23]M. Balkanski, R. F. Wallis, and E. Haro, Phys. Rev. B **28**, 1928 (1983).
[24]B. Song, J. K. Jian, G. Wang, H. Q. Bao, and X. L. Chen, J. Appl. Phys. **101**, 124302 (2007).
[25]E. S. Zouboulis and M. Grimsditch, Phys. Rev. B **43**, 12490 (1991).
[26]J. Menéndez and M. Cardona, Phys. Rev. B **29**, 2051 (1984).
[27]M. Kuball, J. M. Hayes, Y. Shi, and J. H. Edgar, Appl. Phys. Lett. **77**, 1958 (2000).
[28]M. Kazan, Ch. Zgheib, E. Moussaed, and P. Masri, Diamond Relat. Mater. **15**, 1169 (2006).
[29]D. Y. Song, M. Holtz, A. Chandolu, S. A. Nikishin, E. N. Mokhov, Yu. Makarov, and H. Helava, Appl. Phys. Lett. **89**, 021901 (2006).
[30]P. G. Klemens, Physica B **316**, 413 (2002).
[31]J. Z. Zhang, M. Giehle, A. Göbel, T. Ruf, and M. Cardona, Phys. Rev. B **57**, 1348 (1998).
[32]L. E. McNeil, M. Grimsditch, and R. H. French, J. Am. Ceram. Soc. **76**, 1132 (1993).
[33]J. G. Tischler and J. A. Freitas, Jr., Appl. Phys. Lett. **85**, 1943 (2004).
[34]M. Kazan, B. Rufflé, Ch. Zgheib, and P. Masri, Diamond Relat. Mater. **15**, 1525 (2006).
[35]B. M. Epelbaum, C. Seitz, A. Mergel, M. Bickermann, and A. Winnacker, J. Cryst. Growth **265**, 577 (2004).
[36]M. Bickermann, B. M. Epelbaum, P. Heimann, Z. G. Herro, and A. Winnacker, Appl. Phys. Lett. **86**, 131904 (2005).
[37]www.hamptonsci.com/mirrors.htm.
[38]F. Engelbrecht and R. Helbig, Phys. Rev. B **48**, 15698 (1993).
[39]M. Kazan, J. Appl. Phys. **102**, 073532 (2007).
[40]W. Gander and W. Gautschi, BIT **40**, 84 (2000).
[41]L. Bergman, M. Dutta, C. Balkas, R. F. Davis, J. A. Christman, D. Alexon, and R. J. Nemanich, J. Appl. Phys. **85**, 3535 (1999).
[42]R. Loudon, Adv. Phys. **13**, 423 (1964).
[43]L. Filippidis, H. Siegle, A. Hoffmann, C. Thomsen, K. Karch, and F. Bechstedt, Phys. Status Solidi B **198**, 621 (1996).
[44]I. F. Chang, S. S. Mitra, J. N. Plendl, and L. C. Mansur, Phys. Status Solidi **28**, 663 (1968).
[45]R. H. Lyddane, R. G. Sachs, and E. Teller, Phys. Rev. **59**, 673 (1941).
[46]C. Bungaro, K. Rapcewicz, and J. Bernholc, Phys. Rev. B **61**, 6720 (2000).
[47]P. G. Klemens, Phys. Rev. **148**, 845 (1966).
[48]D. W. Posener, Aust. J. Phys. **12**, 184 (1959).
[49]L. Bergman, D. Alexson, P. L. Murphy, R. J. Nemanich, M. Dutta, M. A. Stroscio, C. Balakas, H. Shin, and R. F. Davis, Phys. Rev. B **59**, 12977 (1999).
[50]A. N. Pikhin and A. D. Yas'kov, Sov. Phys. Semicond. **15**, 8 (1981).